Multispecies Trapped-Ion Node for Quantum Networking

I. V. Inlek,* C. Crocker, M. Lichtman, K. Sosnova, and C. Monroe
Joint Quantum Institute and Department of Physics, University of Maryland, College Park, Maryland 20742, USA
(Received 3 February 2017; published 23 June 2017)

Trapped atomic ions are a leading platform for quantum information networks, with long-lived identical qubit memories that can be locally entangled through their Coulomb interaction and remotely entangled through photonic channels. However, performing both local and remote operations in a single node of a quantum network requires extreme isolation between spectator qubit memories and qubits associated with the photonic interface. We achieve this isolation by cotrapping $^{171}Yb^+$ and $^{138}Ba^+$ qubits. We further demonstrate the ingredients of a scalable ion trap network node with two distinct experiments that consist of entangling the mixed species qubit pair through their collective motion and entangling a $^{138}Ba^+$ qubit with an emitted visible photon.

DOI: 10.1103/PhysRevLett.118.250502

Trapped atomic ions are among the most advanced platforms for quantum information networks, hosting qubit memories that are inherently identical and have unrivaled coherence properties. A single node of the network can be realized with a chain of trapped ions, where local entangling gate operations use external control fields that couple the qubit states through their collective motion [1–3]. Edges of the network can then be implemented by photonic entangling operations between select "communication" qubits in separate nodes [4–6]. However, the photonic interface for the communication qubits must not disturb the spectator memory qubits, as even a single resonant photon can destroy the quantum memory. Such isolation is best accomplished by using two different species of atomic ions [7]: one for local processing and memory, the other for communicating with other nodes, as shown in Fig. 1.

Here, we demonstrate each of the ingredients of a multispecies ion trap node for use in a potential quantum network [5,8]. This includes coherent quantum state mapping between memory and communication qubits, and the generation of photonic qubits entangled with the communication qubits. We encode the memory qubits in the $^2S_{1/2}$ ground state hyperfine "clock" levels of $^{171}Yb^+$ atomic ions, $|F=0, m_F=0\rangle \equiv |\Downarrow\rangle$ and $|F=1, m_F=0\rangle \equiv |\Uparrow\rangle$ [14]. As communication qubits, we use the $^2S_{1/2}$ ground state electron spin levels of $^{138}Ba^+$ atomic ions, $|J=1/2, m_J=-1/2\rangle \equiv |\downarrow\rangle$ and $|J=1/2, m_J=+1/2\rangle \equiv |\uparrow\rangle$ [15]. The $^{138}Ba^+$ system features relatively long wavelength photon emission lines (493 and 650 nm), easing the technological requirements for the photonic interfaces and providing the necessary isolation from the $^{171}Yb^+$ resonance at 369 nm. We verify the isolation between these two species by observing that the measured coherence time of $^{171}Yb^+$ qubits (~1.5 s) is not affected by fluorescence or the driving laser light associated with a continuously Doppler cooled $^{138}Ba^+$ qubit a few microns away. With the application of dynamical decoupling pulses, a $^{171}Yb^+$ hyperfine qubit coherence time exceeding 10 min has been reported in a similar setup where a nearby $^{138}Ba^+$ ion is used for sympathetic cooling [16].

We use standard spin-dependent fluorescence collection for the near-perfect single-shot detection of the $^{171}Yb^+$ qubit state [14]. The $^{138}Ba^+$ qubit lacks such an isolated cycling transition, so we detect the $^{138}Ba^+$ qubit state only through averaging many identical experiments (see the Supplemental Material [17] for details). However, this limitation is not debilitating: in the multispecies network architecture, $^{138}Ba^+$ qubits serve only as a link between $^{171}Yb^+$ memory qubits. Once the $^{138}Ba^+$ qubit is mapped to neighboring $^{171}Yb^+$ memories through Coulomb-based

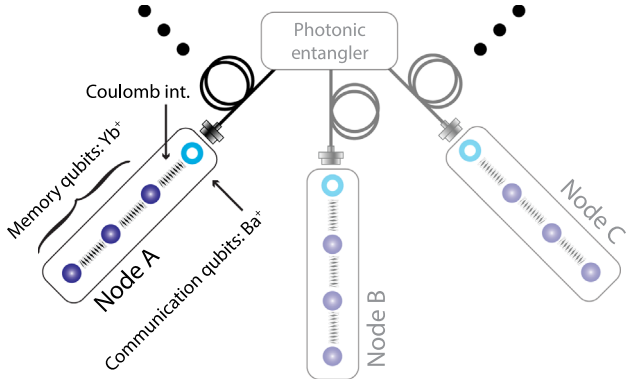

FIG. 1. In an example multispecies ion trap network, $^{138}Ba^+$ communication qubits are coupled to optical fibers. Using photons entangled with their parent atoms, any pair of $^{138}Ba^+$ qubits in different nodes can be entangled through a reconfigurable photonic entangler [8–10]. Local Coulomb interactions mediate transfer of this entanglement to nearby $^{171}Yb^+$ memory qubits [11,12] as well as quantum logic gates within the node [13]. The disparate electronic transition frequencies of the two species provides the necessary isolation to protect $^{171}Yb^+$ memory qubits from resonant processes in the $^{138}Ba^+$ photonic interface.

gates, quantum information processing does not rely on state detection of the $^{138}Ba^{+}$ communication qubits. Nevertheless, the implemented state measurement technique is still useful for a calibration and diagnostics of the $^{138}Ba^{+}$ system.

In addition to their use as photonic communication qubits, $^{138}Ba^{+}$ ions can be employed in sympathetic cooling of $^{171}Yb^{+}$ qubits to maintain occupation in low motional phonon eigenstates for higher fidelity quantum operations. We implement an electromagnetically-induced-transparency (EIT) cooling technique using 493 nm laser beams that are tuned to about 120 MHz blue of the $^{2}S_{1/2}$-$^{2}P_{1/2}$ transition. These beams introduce a narrow atom-laser dressed state resonance where the red-sideband transitions are selectively excited, while blue-sideband and carrier transitions are suppressed [18,19]. With this technique, we cool the motion of a $^{138}Ba^{+}$ and $^{171}Yb^{+}$ two-ion crystal to $\bar{n} \approx 0.06$ (out-of-phase mode) and $\bar{n} \approx 0.1$ (in-phase mode).

Communication qubits do not require long coherence times, as the information can be quickly transferred to memory qubits, where it can be stored and used later. However, the short coherence time of Zeeman $^{138}Ba^{+}$ qubits, due to high magnetic field sensitivity of about 2.8 kHz/mG, might result in errors during transfer operation. We use an arbitrary waveform generator to apply a magnetic field at 60 Hz and higher harmonics with full phase and amplitude control to partially cancel the background field. This technique increases the $^{138}Ba^{+}$ coherence time from 100 μs to approximately 4 ms, which is much longer than any transfer operation gate times.

We demonstrate a photonic interface by entangling the $^{138}Ba^{+}$ qubit with an emitted photon through a postselection procedure [20,21]. Here, in about 1 μs, we initialize the qubit to the $|\downarrow\rangle$ state and weakly excite it to the $^{2}P_{1/2}$ $|J = 1/2, m_J = +1/2\rangle$ level with probability $P_{\text{exc}} \approx 10\%$. We apply 50 μs of Doppler cooling light after 50 entanglement attempts, resulting in an average experimental repetition rate of ~500 kHz. After the excitation, the atom decays back to the $|\downarrow\rangle$ state emitting a σ^{+}-polarized photon, or to the $|\uparrow\rangle$ state emitting a π-polarized photon. We collect the photons perpendicular to the quantization axis; therefore, π photons are registered as vertically polarized in this basis ($|V\rangle$), while σ^{+} photons are registered as horizontally polarized ($|H\rangle$). Given that a photon is collected, this ideally results in an entangled state between the $^{138}Ba^{+}$ qubit and the photon polarization qubit, $|\downarrow\rangle\,|H\rangle + |\uparrow\rangle\,|V\rangle$.

Figures 2(a) and 2(b) show correlation measurements between atom and photon qubit states in multiple bases, and from these measurements we infer the (postselected) entanglement fidelity to be $\mathcal{F} \geq 0.86$. We attribute the errors to polarization mixing due to the large solid angle (10%) [22], multiple photon scattering in the excitation step ($P_{\text{exc}}/4 = 2.5\%$) and imperfect state initialization or detection (1%). These error sources can be significantly reduced

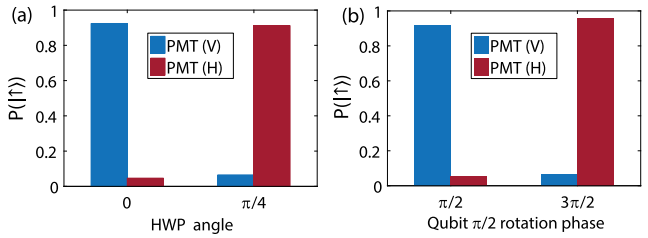

FIG. 2. Correlations between $^{138}Ba^{+}$ qubit and emitted photon polarization in multiple bases. (a) Measured probability of finding a $^{138}Ba^{+}$ qubit in $|\uparrow\rangle$ conditioned upon detecting photon qubit states $|V\rangle$ (light blue) or $|H\rangle$ (dark red) with a photo multiplier tube (PMT). A half wave plate (HWP) rotates the photonic qubit, and the data show two measurements corresponding to HWP angles of 0 and $\pi/4$. (b) The photon polarization is rotated by fixing the HWP at $\pi/8$ so that $|H\rangle \rightarrow |H\rangle - |V\rangle$ and $|V\rangle \rightarrow |H\rangle + |V\rangle$. Subsequent photon detection projects the atom to a superposition $(|\uparrow\rangle + |\downarrow\rangle)|H\rangle + (|\uparrow\rangle - |\downarrow\rangle)|V\rangle$. Following detection of a $|V\rangle$ or $|H\rangle$ photon, we coherently rotate atomic superposition states to $|\downarrow\rangle$ and $|\uparrow\rangle$ with a $\pi/2$ rotation having a phase of either $\pi/2$ or $3\pi/2$, recovering high correlations between the qubit and the photon.

by collecting photons along the quantization axis [10,23] and using pulsed lasers for fast excitation of the atom [9].

Next, we demonstrate a deterministic quantum gate between the two species in the node. We drive coherent Raman transitions in both atomic ions using a single laser for the coherent exchange of information between the $^{171}Yb^{+}$ and $^{138}Ba^{+}$ qubits. We show both a direct Cirac-Zoller (CZ) mapping process by resonantly coupling to the collective motion of the trapped ions [1,11] and a dispersive Mølmer-Sørensen (MS) quantum gate between the qubits [2,12].

We use a Nd:YVO4 mode-locked pulsed laser (Spectra-Physics Vanguard) to introduce noncopropagating Raman beams that can drive transitions between different vibrational eigenmodes and qubit states [24]. As shown in Fig. 3, these beams off-resonantly couple to excited levels: the frequency tripled 355 nm output is used for the $^{171}Yb^{+}$ system, while the frequency doubled 532 nm output from

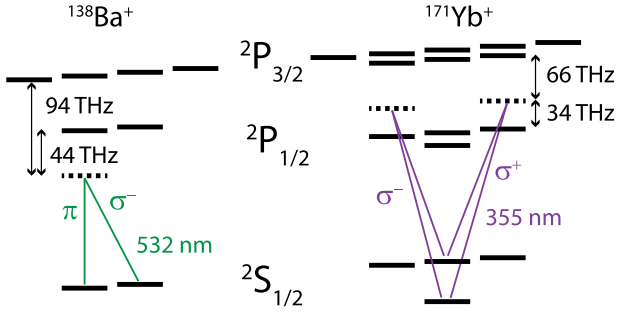

FIG. 3. Off-resonant couplings of 532 and 355 nm pulsed laser beams to $^{2}P_{1/2}$ and $^{2}P_{3/2}$ levels in both $^{138}Ba^{+}$ and $^{171}Yb^{+}$ atomic systems to drive stimulated Raman transitions, with polarizations indicated. The splittings are not to scale.

the same laser is used for the $^{138}Ba^{+}$ system. Stimulated Raman transitions are driven when the beat-note frequency between two beams is near the qubit splitting. We choose linear polarizations that are all perpendicular to the quantization axis, allowing desired Raman transitions to be driven while minimizing differential ac Stark shifts on each species [25]. The large bandwidth of the frequency comb easily spans the $^{171}Yb^{+}$ qubit frequency of 12.642 821 GHz for Raman rotations [26]. In order to stabilize the beat-note frequency of two Raman beams, we use a feed-forward technique that modulates one of the 355 nm beams to compensate for any changes of laser repetition rate [27]. Since the $^{138}Ba^{+}$ qubit splitting is only a few megahertz, we do not rely on multiple comb teeth separation for driving transitions on this qubit; hence, beat-note stabilization is not necessary on 532 nm beams.

While the 355 nm (532 nm) radiation nominally couples only to the $^{171}Yb^{+}$ ($^{138}Ba^{+}$) qubit, there is a small amount of cross-talk coupling to the other atomic system. For equal intensities and without regard to the comb spectrum or the light polarization, the $^{171}Yb^{+}$ system would feel an effective Rabi frequency from the 532 nm radiation that is ~2.6% of the nominal 355 nm radiation Rabi frequency. Likewise, the $^{138}Ba^{+}$ system would feel an ~11% Rabi frequency from the 355 nm radiation. However, the required laser polarization and frequency comb spectrum are different for the two atomic qubit transitions, and we exploit this to reduce cross talk to much less than 1% between the two systems. The spontaneous Raman scattering rate per qubit Rabi cycle is less than 10^{-5} for both atomic species [28], resulting in an error of less than 10^{-5} (10^{-4}) on single (two-) qubit gates. However, rare, spontaneous scattering in the $^{138}Ba^{+}$ system from 532 nm appears to optically pump the $^{138}Ba^{+}$ system through the $^{2}P_{3/2}$ level to the metastable $^{2}D_{5/2}$ state, which has a lifetime of 32 s [29]. We overcome these rare pumping events by illuminating the ions with a diffuse 1 W, orange light-emitting diode (centered around 617 nm) that excites the $^{2}D_{5/2}$ to $^{2}P_{3/2}$ transition at 614 nm with enough intensity to return the ion to the ground state in approximately 30 ms.

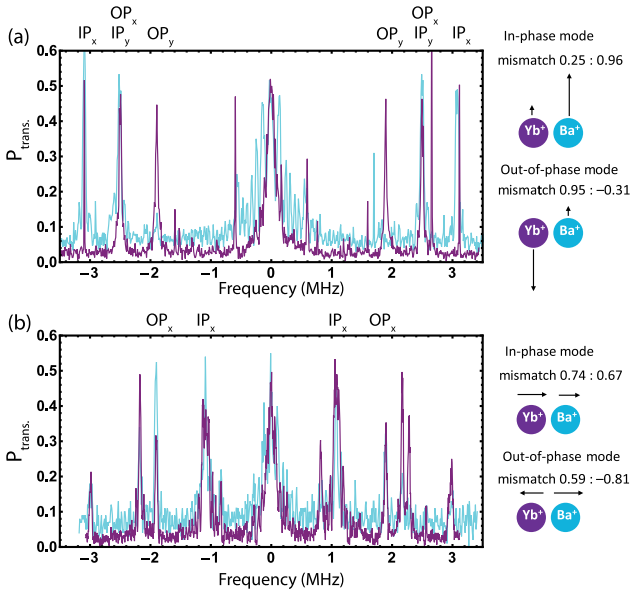

FIG. 4. Raman sideband vibrational spectrum of a cotrapped $^{138}Ba^{+}$–$^{171}Yb^{+}$ crystal is shown for (a) transverse and (b) axial directions of motion. The measured probability of changing the qubit state is plotted in light blue for $^{138}Ba^{+}$ and in dark purple for $^{171}Yb^{+}$, as a function of detuning from the carrier transition where the shared motional phonon state is preserved. The peaks on the positive (negative) values correspond to a blue- (red-) sideband transition in which the spin flip is accompanied by the addition (subtraction) of a phonon [24]. The sidebands corresponding to the in-phase (IP) and out-of-phase (OP) are labeled for the transverse (x, y) and axial (z) directions of motion, with their theoretical eigenvector amplitudes indicated at the right. The unlabeled peaks correspond to higher order sidebands, and interactions involving multiple modes such as subtraction of a phonon from one mode and addition in another.

Despite their similar atomic masses, the transverse motion of a coupled pair of $^{138}Ba^{+}$ and $^{171}Yb^{+}$ ions exhibits a large mismatch in their amplitude for a given mode [7], resulting in a smaller motional coupling between the ions [Fig. 4(a)]. For this reason, we instead use the better-matched axial modes [Fig. 4(b)]. We note that, as the number of ions in the crystal chain increases, the motional eigenvector mismatch in the transverse modes becomes less significant and these modes can be used conveniently to benefit from higher mode frequencies [30].

We first transfer the qubit state of $^{138}Ba^{+}$ to $^{171}Yb^{+}$ by directly using the collective motion in a CZ scheme [1,11]. The procedure [Fig. 5(a)] starts with EIT cooling and preparation of the $^{138}Ba^{+}$ spin state with a carrier transition. Next, a red-sideband π rotation on the $^{138}Ba^{+}$ system

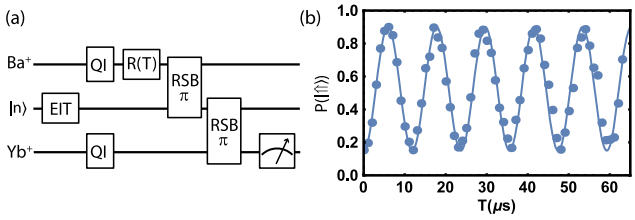

FIG. 5. (a) Experimental steps on mapping the state of $^{138}Ba^{+}$ to $^{171}Yb^{+}$ using collective motion directly. The procedure starts with EIT cooling, followed by the initialization of qubit states (QI) to $|\downarrow\rangle$ and $|\Downarrow\rangle$. Afterwards, a stimulated Raman rotation $R(T)$ of the $^{138}Ba^{+}$ qubit over time T prepares the state to be transferred. A red-sideband π rotation (RSB π) on the $^{138}Ba^{+}$ qubit transfers this information to shared phonon mode, which is then transferred to the $^{171}Yb^{+}$ qubit with another red-sideband π rotation. In the final step, the $^{171}Yb^{+}$ qubit state is measured. (b) The data show the probability of finding a $^{171}Yb^{+}$ qubit in $|\Uparrow\rangle$ as a function of the $^{138}Ba^{+}$ qubit rotation time T, with an observed state transfer efficiency of ≈0.75.

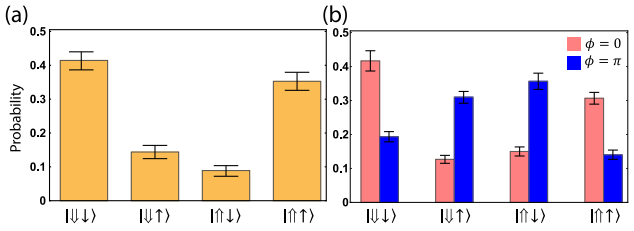

FIG. 6. (a) Measured probabilities of the $^{171}Yb^{+}$ and $^{138}Ba^{+}$ qubit states after an entangling MS gate is applied to the initial $|\Downarrow\downarrow\rangle$ state. This interaction would ideally create the maximally entangled $(1/\sqrt{2})(|\Downarrow\downarrow\rangle - e^{-i\phi_S}|\Uparrow\uparrow\rangle)$ state. The optical phases of the driving fields are imprinted on spins with the gate phase, ϕ_S. (b) Following the MS interaction, $\pi/2$ rotations are applied to both qubits. The phase of $^{138}Ba^{+}$ $\pi/2$ pulse is kept constant, while the $^{171}Yb^{+}$ $\pi/2$ rotation phase is scanned. The data show measured qubit state probabilities at the maximum parity points $|P(|\Downarrow\downarrow\rangle) + P(|\Uparrow\uparrow\rangle) - P(|\Downarrow\uparrow\rangle) - P(|\Uparrow\downarrow\rangle)|$.

transfers information to a shared phonon mode, which is then transferred to the $^{171}Yb^{+}$ qubit with a further red-sideband π rotation on the $^{171}Yb^{+}$ system. The overall state transfer efficiency of 0.75, as shown in Fig. 5(b), was limited primarily by the purity of the initial motional state. But the main drawback to the CZ method is the necessity of phase coherence between the communication qubit and the CZ mapping operations. Because the communication qubit may have prior entanglement through the photonic channel, the CZ mapping method requires stabilizing the beam paths to much better than an optical wavelength.

We next demonstrate a Mølmer-Sørensen transfer method that relaxes the above limitations. In the MS transfer scheme [12,31], entanglement and state transfer fidelity require only confinement to the Lamb-Dicke limit [24], which we achieve with 300 μs of Doppler cooling followed by 500 μs of EIT cooling. A MS entangling gate is realized in our system by simultaneously addressing the axial out-of-phase mode with a symmetric detuning δ using pairs of noncopropagating Raman beams. Since the pulse pairs of 355 and 532 nm follow different paths, they are not necessarily incident on the atoms at the same time. Importantly, a temporal overlap between these pairs is not necessary for the MS interaction; spin-dependent forces using the Raman beams can be applied at different times to each atom. The outcome is just a static phase on the entangled state which can be controlled by adjusting either the optical path lengths or the difference between rf beat-note phases of the 355 and 532 nm driving fields. These spin-dependent forces displace the motional wave packets of certain two-qubit states in phase space. We incorporate Walsh modulation to suppress frequency and timing errors [32], and, after a gate time $T = 200$ μs with a detuning of $\delta = 10$ kHz, the motion returns to its original state, picking up a geometrical phase as in the usual MS gate [33]. The optical intensities of the driving fields are adjusted to obtain carrier Rabi frequencies of $\Omega = \delta/4\eta$ to result in a $\pi/2$ geometrical phase after the MS interaction, where η is the Lamb-Dicke parameter [12]. We find the correct optical force phase by monitoring the acquired geometrical phases. To maintain a shot-to-shot relative optical force phase, we use the same arbitrary waveform generator to drive acousto-optic modulators for 355 and 532 nm beams. The fidelity of this operation is approximately $\mathcal{F} = 0.60$, as shown in Fig. 6, and we attribute this low fidelity to excessive heating ($\dot{\bar{n}} \approx 5$ ms^{-1}) of the axial out-of-phase mode [33].

Even though the phases of the optical fields are imprinted on the entangled state after this interaction, two consecutive MS gates with a relative π phase difference can be used to coherently transfer the information from communication to memory qubit without imprinting an extra optical phase (see the Supplemental Material [17] and Ref. [34] for details). Thus, phase coherence between remote and local entanglement operations in the quantum network can be established without a need for directly eliminating optical phase dependence from the MS gate with extra single qubit operations [12,35] or special beam geometries [36].

Based on the tools demonstrated in this Letter, we can extend a quantum network to many nodes using photonic Bell state analyzers to make the photonic connections. We expect that considerable improvements on the atom-photon and atom-atom entanglement fidelities and rates are possible in order to scale to many interconnected nodes. First, the encoding of photonic qubits into two different frequencies rather than into polarization is expected to provide significant improvements in the remote communication qubit fidelity [37]. Second, the use of fabricated chip traps with integrated optical elements [38] is expected to enhance the connection rate between nodes. Additionally, the positional stability of the ions stemming from the uniformity and repeatability of construction, as well as heating rates comparable to hand-assembled traps (such as the Sandia National Laboratories high-optical-access microfabricated ion trap with $\dot{\bar{n}} < 40$ s^{-1} [39]), would likely allow for much higher fidelity motional gates between memory and communication qubits in these fabricated traps.

We acknowledge the useful discussions with D. Hucul and G. Vittorini. This work was supported by the ARO with funds from the IARPA MQCO and LogiQ programs, the AFOSR MURI on Quantum Measurement and Verification, the AFOSR MURI on Quantum Transducers, the ARL Center for Distributed Quantum Information, and the National Science Foundation Physics Frontier Center at JQI.

*volkan.inlek@duke.edu
Present address: Department of Electrical and Computer Engineering, Duke University, Durham, NC 27708, USA.

[1] J. I. Cirac and P. Zoller, Phys. Rev. Lett. **74**, 4091 (1995).
[2] A. Sørensen and K. Mølmer, Phys. Rev. A **62**, 022311 (2000).

[3] R. Blatt and D. Wineland, Nature (London) **453**, 1008 (2008).
[4] H. J. Kimble, Nature (London) **453**, 1023 (2008).
[5] L.-M. Duan and C. Monroe, Rev. Mod. Phys. **82**, 1209 (2010).
[6] N. H. Nickerson, Y. Li, and S. C. Benjamin, Nat. Commun. **4**, 1756 (2013).
[7] J. P. Home, Adv. At. Mol. Opt. Phys. **62**, 231 (2013).
[8] C. Monroe, R. Raussendorf, A. Ruthven, K. R. Brown, P. Maunz, L.-M. Duan, and J. Kim, Phys. Rev. A **89**, 022317 (2014).
[9] D. L. Moehring, P. Maunz, S. Olmschenk, K. C. Younge, D. N. Matsukevich, L.-M. Duan, and C. Monroe, Nature (London) **449**, 68 (2007).
[10] D. Hucul, I. V. Inlek, G. Vittorini, C. Crocker, S. Debnath, S. M. Clark, and C. Monroe, Nat. Phys. **11**, 37 (2015).
[11] P. O. Schmidt, T. Rosenband, C. Langer, W. M. Itano, J. C. Bergquist, and D. J. Wineland, Science **309**, 749 (2005).
[12] T. R. Tan, J. P. Gaebler, Y. Lin, Y. Wan, R. Bowler, D. Leibfried, and D. J. Wineland, Nature (London) **528**, 380 (2015).
[13] S. Debnath, N. M. Linke, C. Figgatt, K. A. Landsman, K. Wright, and C. Monroe, Nature (London) **536**, 63 (2016).
[14] S. Olmschenk, K. C. Younge, D. L. Moehring, D. N. Matsukevich, P. Maunz, and C. Monroe, Phys. Rev. A **76**, 052314 (2007).
[15] A. Kleczewski, M. R. Hoffman, J. A. Sherman, E. Magnuson, B. B. Blinov, and E. N. Fortson, Phys. Rev. A **85**, 043418 (2012).
[16] Y. Wang, M. Um, J. Zhang, S. An, M. Lyu, J.-N. Zhang, L.-M. Duan, D. Yum, and K. Kim, arXiv:1701.04195.
[17] See Supplemental Material at http://link.aps.org/supplemental/10.1103/PhysRevLett.118.250502 for $^{138}Ba^{+}$ qubit state detection, and phase considerations in the quantum networks.
[18] Y. Lin, J. P. Gaebler, T. R. Tan, R. Bowler, J. D. Jost, D. Leibfried, and D. J. Wineland, Phys. Rev. Lett. **110**, 153002 (2013).
[19] G. Morigi, Phys. Rev. A **67**, 033402 (2003).
[20] B. B. Blinov, D. L. Moehring, L.-M. Duan, and C. Monroe, Nature (London) **428**, 153 (2004).
[21] C. Auchter, C.-K. Chou, T. W. Noel, and B. B. Blinov, J. Opt. Soc. Am. B **31**, 1568 (2014).
[22] S. M. Olmschenk, Ph.D. thesis, University of Michigan, 2009.
[23] T. Kim, P. Maunz, and J. Kim, Phys. Rev. A **84**, 063423 (2011).
[24] D. Leibfried, R. Blatt, C. Monroe, and D. Wineland, Rev. Mod. Phys. **75**, 281 (2003).
[25] A. C. Lee, J. Smith, P. Richerme, B. Neyenhuis, P. W. Hess, J. Zhang, and C. Monroe, Phys. Rev. A **94**, 042308 (2016).
[26] D. Hayes, D. N. Matsukevich, P. Maunz, D. Hucul, Q. Quraishi, S. Olmschenk, W. Campbell, J. Mizrahi, C. Senko, and C. Monroe, Phys. Rev. Lett. **104**, 140501 (2010).
[27] R. Islam *et al.*, Opt. Lett. **39**, 3238 (2014).
[28] W. C. Campbell, J. Mizrahi, Q. Quraishi, C. Senko, D. Hayes, D. Hucul, D. N. Matsukevich, P. Maunz, and C. Monroe, Phys. Rev. Lett. **105**, 090502 (2010).
[29] C. Auchter, T. W. Noel, M. R. Hoffman, S. R. Williams, and B. B. Blinov, Phys. Rev. A **90**, 060501 (2014).
[30] S.-L. Zhu, C. Monroe, and L.-M. Duan, Phys. Rev. Lett. **97**, 050505 (2006).
[31] C. J. Ballance *et al.*, Nature (London) **528**, 384 (2015).
[32] D. Hayes, S. M. Clark, S. Debnath, D. Hucul, I. V. Inlek, K. W. Lee, Q. Quraishi, and C. Monroe, Phys. Rev. Lett. **109**, 020503 (2012).
[33] A. Sørensen and K. Mølmer, Phys. Rev. A **62**, 022311 (2000).
[34] I. V. Inlek, Ph.D. thesis, University of Maryland, 2016.
[35] P. J. Lee, K.-A. Brickman, L. Deslauriers, P. C. Haljan, L.-M. Duan, and C. Monroe, J. Opt. B **7**, S371 (2005).
[36] I. V. Inlek, G. Vittorini, D. Hucul, C. Crocker, and C. Monroe, Phys. Rev. A **90**, 042316 (2014).
[37] S. Olmschenk, D. N. Matsukevich, P. Maunz, D. Hayes, L.-M. Duan, and C. Monroe, Science **323**, 486 (2009).
[38] A. van Rynbach, P. Maunz, and J. Kim, Appl. Phys. Lett. **109**, 221108 (2016).
[39] P. Maunz, Sandia National Laboratories (SNL-NM), Albuquerque, NM Report No. SAND2016-0796R.